ARTICLE

Dip-Pen Nanolithography of Electrical Contacts to Single-Walled Carbon Nanotubes

Wechung Maria Wang,[†] Melburne C. LeMieux,[†] Selvapraba Selvarasah,[‡] Mehmet R. Dokmeci,[‡] and Zhenan Bao[†,*]

[†]Department of Chemical Engineering, Stanford University, Stanford, California 94305 and [‡]Department of Electrical and Computer Engineering, Northeastern University, Boston, Massachusetts 02115

ABSTRACT This paper discusses a method for the direct patterning of Au electrodes at nanoscale resolution using dip-pen nanolithography, with proof-of-concept demonstrated by creating single-walled carbon nanotube devices. This technique enables insight into three key concepts at the nanoscale: using dip-pen nanolithography as an alternative to electron-beam lithography for writing contacts to carbon nanotubes, understanding the integrity of contacts and devices patterned with this technique, and on a more fundamental level, providing a facile method to compare and understand electrical and Raman spectroscopy data from the same isolated carbon nanotube. Electrical contacts to individual and small bundle single-walled carbon nanotubes were masked by an alkylthiol that was deposited *via* dip-pen nanolithography on a thin film of Au evaporated onto spin-cast, nonpercolating, and highly isolated single-walled carbon nanotubes. A wet Au etching step was used to form the individual devices. The electrical characteristics for three different single-walled carbon nanotube devices are reported: semimetallic, semiconducting, and metallic. Raman analysis on representative devices corroborates the results from AFM imaging and electrical testing. This work demonstrates a technique for making electrical contact to nanostructures of interest and provides a platform for directly corroborating electrical and optical measurements. The merits of using dip-pen nanolithography include flexible device configuration (such as varying the channel length and the number, size, and orientation of contacts), targeted patterning of individual devices with imaging and writing conducted in the same instrument under ambient conditions, and negligible damage to single-walled carbon nanotubes during the fabrication process.

KEYWORDS: gold electrode · patterning · carbon nanotube · scanning probe lithography · dip-pen nanolithography · nanofabrication

Single-walled carbon nanotubes (SWNTs) have demonstrated their unique electrical properties as components in single-electron[1] and field-effect transistors,[2−4] chemical sensors,[5−7] and transparent electronics.[8−10] Engineeringthese carbon nanotube-based devices requires further fundamental studies on SWNT charge transport properties[11,12] and their dependence on device configuration.[13] The conventional method of fabricating single nanotube devices for such studies has been electron-beam lithography;[2,14−16] however, exposure to electron irradiation can damage SWNTs,[17−21] thereby preventing measurement of intrinsic properties. This paper introduces an alternative method for fabricating SWNT devices *via* dip-pen nanolithography (DPN), a scanning probe-based technique that combines the nanoscale resolution of electron-beam lithography with the direct-write capability of microcontact printing.[22,23] The versatility of DPN is evidenced by its wide range of inks, such as the seminal and widely used alkanethiols,[24−27] conducting polymers,[28−30] biological molecules,[31−35] and metal nanoparticles.[36−41] This work applies DPN toward patterning electrical contacts in nanoelectronic devices. The advantages of such an approach include selective placement and design of electrical contacts, targeted device fabrication (*versus* random selection as in electron-beam lithography of predefined contacts), minimal damage during the fabrication process (no electron irradiation), and imaging SWNTs and patterning contacts in one system under ambient conditions.

DPN of 16-mercaptohexadecanoic acid (MHA) has been used to generate an etch-resist layer on Au films for patterning Au nanostructures on silicon.[42−48] This paper optimizes the aforementioned MHA-masking method toward fabricating Au contacts to arbitrary arc-discharge SWNTs. Arc-discharge SWNTs were used due to their bulk production and solution processability being relevant to electronic applications. Au was used as the electrically contacting material and has been shown to make ohmic contact to carbon nanotubes operating as p-type transistors.[49] MHA remains on the Au contacts after fabrication and may affect the electrical characteristics of SWNT devices;[50] however, the MHA may be removed by annealing the substrate at sufficiently high temperatures[51] or by

*Address correspondence to zbao@stanford.edu.

Received for review August 11, 2009 and accepted October 19, 2009.

Published online October 23, 2009.
10.1021/nn900984w CCC: $40.75

© 2009 American Chemical Society

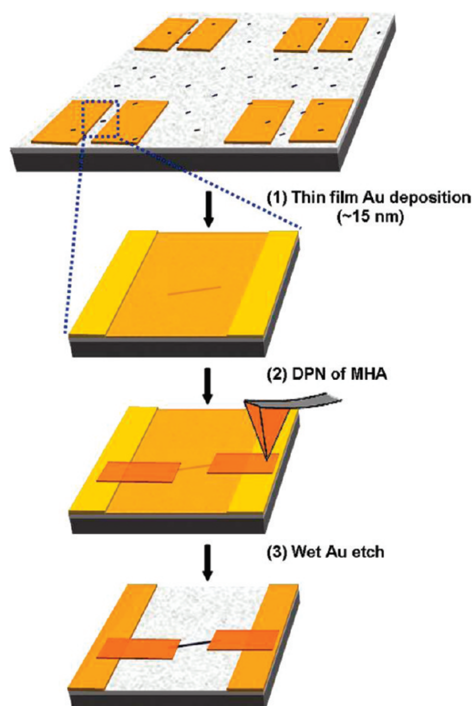

Figure 1. Schematic of SWNT device fabrication. The substrate is prepared by spin-casting a dilute solution of SWNTs onto SiO_2/Si functionalized with an aminosilane to promote absorption. (1) A thin film of Au (~15 nm) is thermally evaporated onto the substrate, either on top of photolithographically patterned Au electrodes (as shown) or under Au electrodes to be patterned *via* a parylene-C shadow mask. (2) An AFM tip inked with MHA is used for rapid imaging of the SWNTs under the thin film of Au and eventually masking contacts to the ends of an arbitrary SWNT. (3) The substrate is immersed in a wet Au etchant to form the SWNT device.

exposure to a $NaBH_4$ solution.[52] This straightforward device fabrication technique (Figure 1) allows for electrical measurements on SWNTs with various dimensions and chiralities.

The challenges in developing this method included optimization of the Au film, making it thick enough to be conductive yet thin enough so that AFM scanning could detect the SWNTs underneath. Furthermore, the diffusivity of MHA was optimized to obtain reliable patterns for electrical contacts (e.g., no shorts, clean etch), and two types of Au etchant were evaluated for comparison of etch quality. Challenges in forming reliable electrical contact between the MHA-masked Au and the larger Au electrodes used for electrical probe measurements led to development of two device fabrication routes. Finally, electrical characterization and Raman analysis of different types of SWNT devices were conducted to validate this fabrication method.

RESULTS AND DISCUSSION

MHA Diffusivity. A typical substrate for DPN is shown in Figure 2: the channel lengths to be bridged by MHA-masked contacts are 5 to 10 μm. The lateral force microscopy (LFM) image shows rectangular MHA patterns overlapping the ends of the SWNT and the larger Au

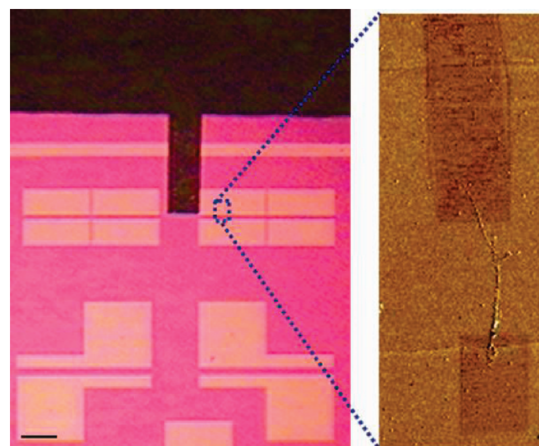

Figure 2. (left) Optical image of a substrate with electrically isolated SWNTs and predefined Au electrodes beneath a thin film of Au. The area to be patterned by DPN is denoted with a blue circle. Scale bar is 40 μm. (right) LFM image of a SWNT after MHA masking of contacts to the predefined Au electrodes.

electrodes across a 5 μm channel. These boundary patterns were created using InkCAD software, which allowed for the specification of feature sizes based on MHA diffusivity calculated at the beginning of each patterning session *via* a calibration tool built into InkCAD. The optimal range of MHA diffusivity was found to be 0.02−0.05 μm^2/s. For diffusivity lower than 0.02 μm^2/s, the long patterning time resulted in vapor diffusion of MHA indiscriminately onto the substrate surface. For diffusivity higher than 0.05 μm^2/s, the patterns were not well-defined and often resulted in shorted devices, possibly due to formation of multilayers of MHA during patterning and/or deposition during scanning. The time required for DPN of a single device was 5−20 min, depending on channel length and contact configuration. In cases where carbon nanotubes operate as Schottky barrier transistors, the conductance can be modulated by the electric field at the contacts; therefore, the contact geometry can be optimized, for example, designed to be sharper and thinner, to improve device performance.[53]

Au Etchant Selectivity. After patterning the MHA-masking layer, the substrates were exposed to a gold etchant (details in Methods section). Two types of wet etchants that have been used for Au patterned with self-assembled monolayers (SAMs)[44,54] were evaluated for their selectivity in preserving the MHA-masked Au. As shown in Figure 3, the ferric nitrate/thiourea etchant yielded a cleaner etch (fewer residual Au particles) and better pattern fidelity than the ferri/ferrocyanide etchant. The Au contacts in Figure 3a are less uniform and have a higher pinhole density compared to those in Figure 3b (see height profile insets). The SAM mask may have been undermined by the slower etch rate of ferri/ferrocyanide (~0.7 nm/min) compared to ferric nitrate/thiourea (~2.5 nm/min). Moreover, the charged thiosulfate species in the ferri/ferrocyanide etchant is

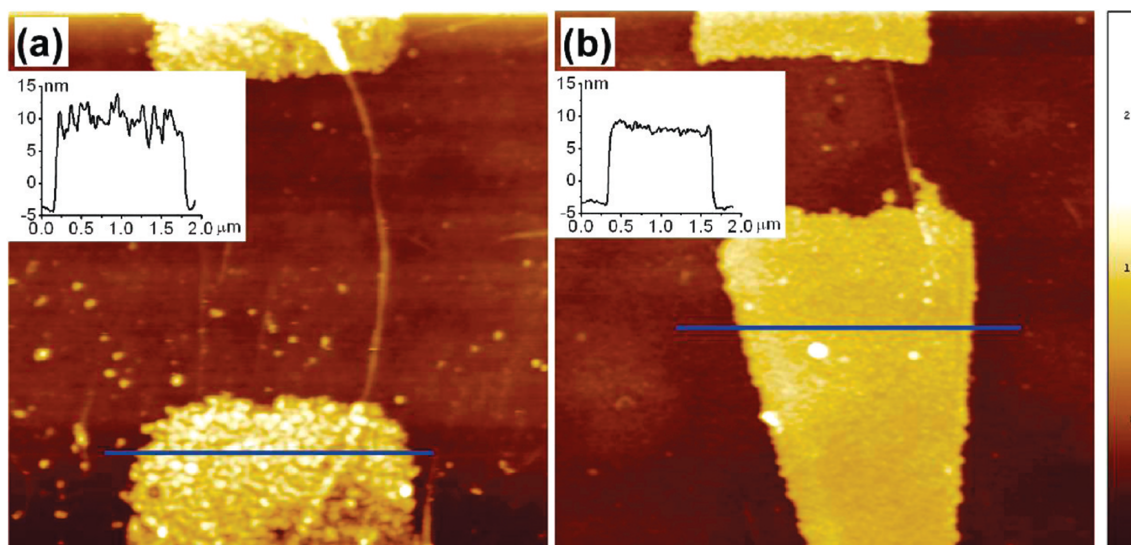

Figure 3. AFM topography images of MHA-masked Au contacts to SWNTs after etching in ferri/ferrocyanide (a) and ferric nitrate/thiourea (b). The blue lines denote line profiles of the height variation, shown in the insets.

more likely to penetrate the hydrated surface of the MHA SAM than the neutral thiourea species.[55] The higher selectivity of the ferric nitrate/thiourea etch led to its use in producing subsequent SWNT devices. Figure 4 shows different contact configurations to SWNTs after etching with ferric nitrate/thiourea. These patterns demonstrate the versatility of DPN in designing contact configurations for specific types of SWNTs (*e.g.*, depending on their orientation, size, single SWNT or junctions).

Quality of Au Contacts. The MHA-defined Au served as electrical contacts between the ends of SWNTs and the larger Au electrodes, which were either photolithographically patterned under SWNTs and a thin film of Au (as shown in Figure 2) or deposited *via* a parylene-C shadow mask[56] on top of the thin film of Au. The photolithographically patterned Au electrodes were fabricated on a wafer scale and could be stored for future use when a fresh film of Au would be deposited on top for DPN. However, there were disadvantages to using the photolithographically patterned Au electrodes. First, depositing a thin film of Au (10−15 nm) on top of thicker, predefined electrodes (35−40 nm) resulted in a discontinuity at the electrode edges due to the height barrier. Therefore, if the predefined electrodes were to be under the Au thin film, both depositions needed to be of similar thickness (15−17 nm, thin enough to image SWNTs underneath) and thermal annealing was required to obtain consistent conductivity. Furthermore, careful probing during electrical measurement was necessary so as not to pierce through the thin Au electrodes. Depositing the Au electrodes

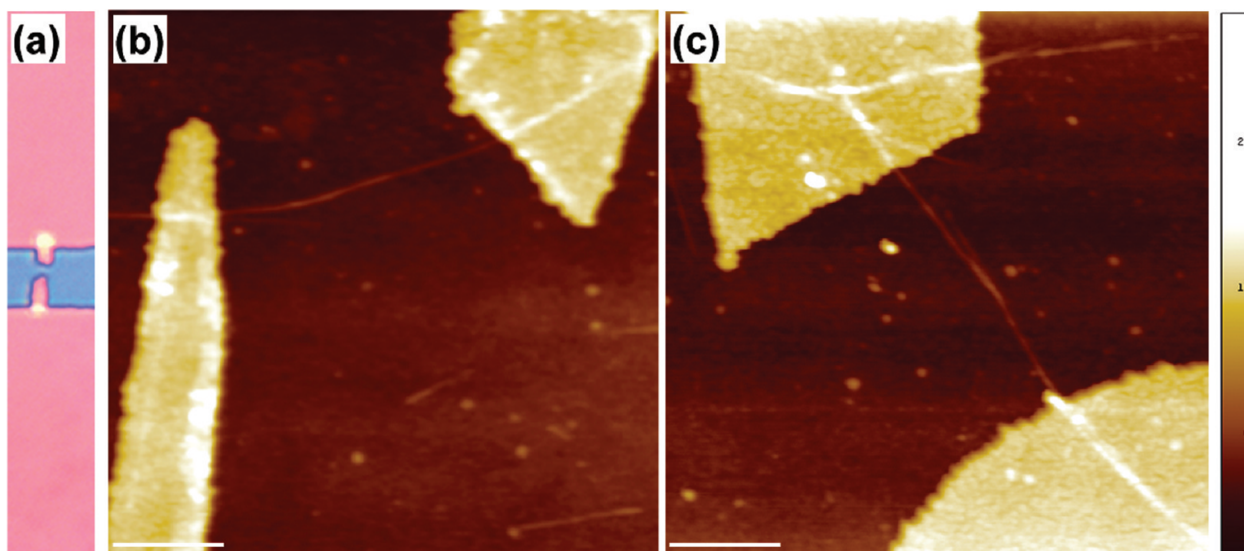

Figure 4. (a) Optical image of a SWNT device. The distance between the larger Au pads is 5 μm. (b,c) AFM topography images of MHA-masked Au contacts to a single SWNT and a junction of two single SWNTs, respectively. Scale bars are 500 nm.

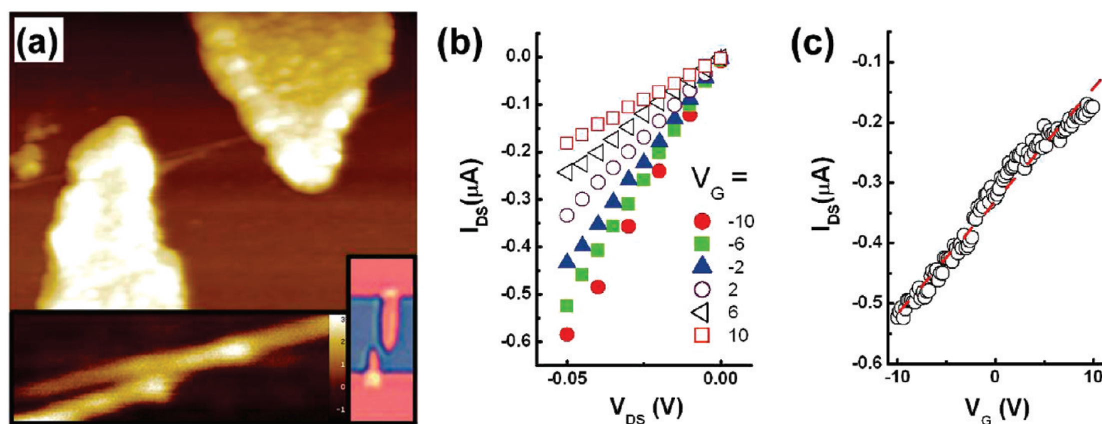

Figure 5. (a) AFM topography image of a semimetallic SWNT device with the two-tube bundle magnified in the inset (Z-scale is 3 nm), which also shows the optical image of the entire device. The length of the SWNT section between the MHA-masked Au contacts is 600 nm. (b) Output curves indicating semimetallic behavior. (c) Transfer curve at $V_{DS} = -0.05$ V and sweeping from −10 to 10 V. The dashed red line denotes a linear fit for calculating the transconductance.

through a parylene-C shadow mask on top of the Au thin film circumvented these limitations. Moreover, if one end of a SWNT was already under an electrode, then only one top contact needed to be patterned with DPN, thereby halving the patterning time per device. The conductivity of the MHA-masked Au contacts ranged from ~4 to 5 × 10^6 S/m (refer to Supporting Information, Figure S1), which is the same as that measured for Au nanostructures fabricated *via* electron-beam lithography.[57] Therefore, DPN is a comparable substitute for electron-beam lithography in creating conductive Au contacts for nanostructured devices.

SWNT Devices. Besides ensuring that the DPN-generated contacts were conductive, it was necessary to show that this fabrication process did not damage the SWNTs. Therefore, a more concentrated (10×) SWNT solution was used to prepare a percolating network of SWNTs as thin-film field-effect transistors, which were then subjected to the same processing conditions of Au deposition and subsequent etching. Electrical characterization of these devices before and after processing yielded similar *I*−*V* characteristics (refer to Supporting Information, Figure S2), thereby demonstrating that this fabrication method does not alter the electronic properties of SWNTs and suggesting that the SWNTs have not been damaged.

The functionality of DPN-patterned devices was verified through electrical measurements on three different types of SWNTs: semimetallic, semiconducting, and metallic. To compare the performance of these devices with those reported in the literature, key figures of merit were calculated, such as the transconductance ($g_m = dI_{DS}/dV_G$) at a given source-drain voltage (V_{DS}) and the field-effect mobility for operation in the linear regime: $\mu = (L/V_{DS}C_t)(dI_{DS}/dV_G)$, where L is the device channel length between the MHA-masked Au contacts and C_t is the gate capacitance per unit length of the SWNT, estimated from $2\pi\varepsilon_{ox}/\ln(4t_{ox}/W)$, where ε_{ox} is the effective dielectric constant of SiO_2 ($3.9\varepsilon_0$), t_{ox} is the oxide thickness (300 nm), and W is the diameter of the SWNT.[2]

A semimetallic SWNT device is shown in Figure 5; the device did not turn off, even at $V_G = 10$ V, yet the measured current was modulated by V_G. The AFM image reveals that this device consists of two nanotubes in a y-shaped junction. The calculated transconductance was 1.9 × 10^{-8} S, which is an order of magnitude greater than that reported in literature for a single solution-processed SWNT with a similar device structure (SiO_2/Si substrate with Au electrodes) fabricated *via* electron-beam lithography.[2] The higher transconductance may be due to this device being a two-tube bundle.

Figure 6 shows the measured *I*−*V* curves for the p-type semiconducting SWNT in Figure 2. The on/off ratio was ~4000, and leakage current was in the picoamp range with no dependence on V_G. The field-effect mobility was ~23 $cm^2/V\cdot s$ ($W = 2$ nm, $L = 2$ μm), which is within the same order of magnitude as reported for solution-processed, single SWNTs in the literature,[2,58] as is the transconductance at 3.6 × 10^{-9} S.

Another p-type semiconducting SWNT device is shown in Figure 7. The residual Au seen in the AFM image is from an incomplete etch; the exposure time was not long enough to etch all of the unmasked Au film, possibly due to a measurement error in the thickness of the Au for that particular deposition. Nevertheless, the calculated figures of merit for this device are within the same order of magnitude as previous ones ($g_m = 5.9 \times 10^{-9}$ S and $\mu \approx 67$ $cm^2/V\cdot s$ for $W = 1.6$ nm, $L = 1.86$ μm). The $I_{DS,max}$ for this single SWNT device is much lower than for the bundle in Figure 5. Furthermore, repeated electrical measurements resulted in loss of conductivity probably due to breakdown of the tube.[59] Indeed, AFM imaging after additional Au etching revealed that a gap formed along the SWNT (inset in Figure 9c).

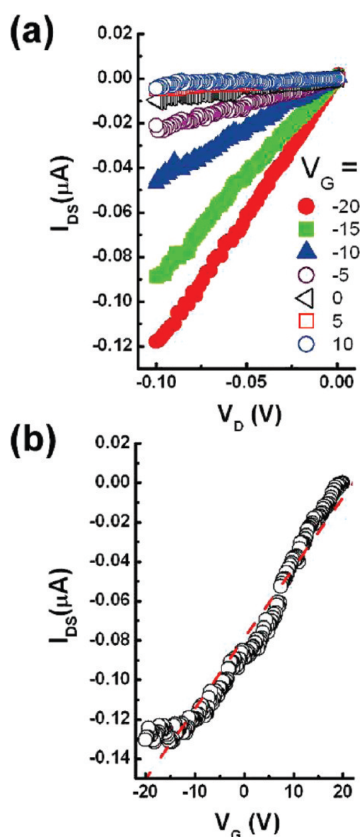

Figure 6. Output (a) and transfer (b) curves for the SWNT device shown in Figure 2, indicating p-type semiconducting behavior. The dashed red line denotes a linear fit for calculating the transconductance at $V_{DS} = -0.1$ V as V_G sweeps from 20 to −20 V.

A metallic SWNT device is shown in Figure 8. The current was not modulated by V_G, and the measured resistance was 130 kΩ, which is comparable to that measured in devices with low-resistance contacts fabricated *via* electron-beam lithography.[60] Further evidence for the MHA-masked Au as low-resistance contacts is presented in Supporting Information, Figure S3, which shows a short-channel metallic SWNT device ($L = 135$ nm) with a resistance of ~18 kΩ at room temperature, indicating that the MHA-masked Au is likely making

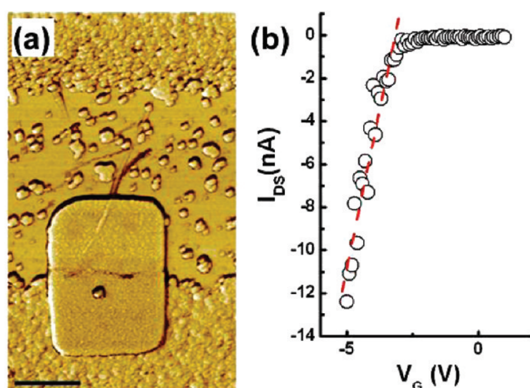

Figure 7. (a) AFM phase image of a semiconducting SWNT device. Scale bar is 1 μm. (b) Transfer curve at $V_{DS} = -0.05$ V and sweeping from −5 to 1 V. The dashed red line denotes a linear fit for calculating the transconductance.

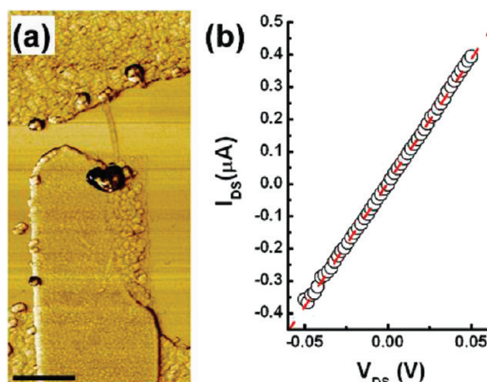

Figure 8. (a) AFM phase image of a metallic SWNT device. Scale bar is 1 μm. (b) Corresponding *I*−*V* curve. The dashed red line denotes a linear fit for calculating the resistance.

ohmic contact to the SWNT.[11,49] Therefore, this technique can potentially be used to probe the intrinsic electrical properties of SWNTs. The majority of the SWNT devices patterned *via* DPN in this study were composed of bundles or metallic tubes because these were easier to locate under the Au thin film due to their mostly larger diameters when compared to individual semiconducting SWNTs. The yield of devices under optimized conditions was 60%, with the nonfunctional devices due to alignment error or overetching of Au contacts at the edges of the substrate.

Raman Analysis. To complement the electrical characterization, Raman data obtained from high-resolution spectral mapping of the SWNT devices were analyzed. The DPN-patterned devices were easily identified through optics in the Raman system, resulting in a very high probability of analyzing the specific SWNTs in the device channels. This attribute of the DPN-patterned electrodes is advantageous for the difficult experiment of obtaining electrical, topographical, and optical (structural) data from the same isolated nanotube. The conventional method of conducting such studies has involved using a more complicated experimental setup such as low-temperature scanning tunneling microscopy and scanning tunneling spectroscopy.[61,62] Moreover, DPN offers the flexibility of writing to only the species of interest, in this case an individual tube and a bundle that exhibited different electronic properties, thereby providing a versatile method for comparing and understanding fundamental properties of nanotubes. Although directly correlated electrical and Raman measurements have been conducted previously on the same nanotube species, these studies lacked AFM topographical data[63] or were conducted on a single double-walled nanotube[64] or nanotube films.[65,66] Recently, a method for directly correlating electrical and Raman data was reported for isolated nanotubes,[67] but it involved transfer printing CVD-grown tubes onto a substrate with predefined electrodes, thereby lacking the flexibility of direct imag-

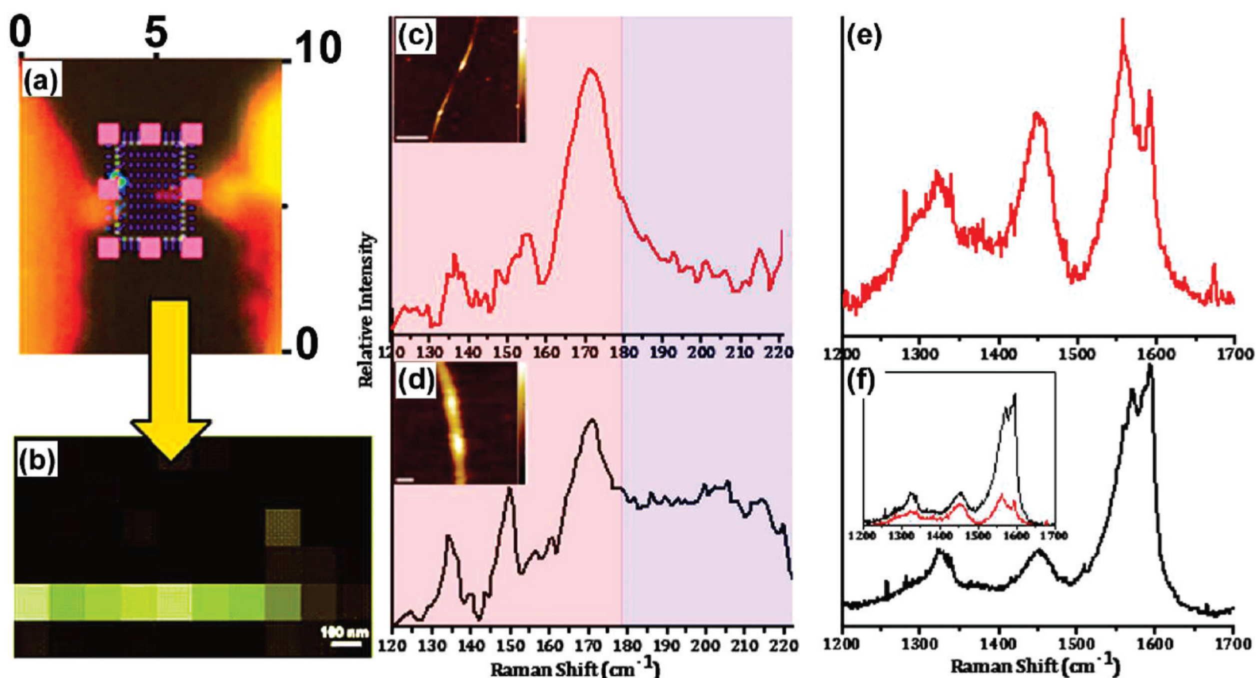

Figure 9. Raman spectral mapping of the DPN-patterned devices at 633 nm compiled from 10 × 10 (100 point) mapping. (a) Optical image (100×), with mapping points overlaid, of a typical DPN-patterned device for Raman characterization, with the scale in units of micrometers. The isolated nanotube bridges the gap between the MHA-masked Au at the closest point. (b) Resulting map image of the nanotube on the Si substrate, with contrast resulting from the intensity difference at ~1600 cm^{-1} (G-band) between a spot with a nanotube or only Si (no peak at 1600 cm^{-1}). Scale bar is 100 nm. (c) Compiled average spectra in the RBM region of an individual semiconducting SWNT (pink and purple shading represent semiconducting and metallic transitions, respectively), along with AFM image (inset, scale bar is 500 nm, Z-scale is 5 nm). (d) Compiled average spectra in the RBM region of an isolated nanotube bundle displaying both semiconducting and metallic peaks, along with AFM image (inset, scale bar is 100 nm, Z-scale is 4 nm). (e,f) G-band region of the individual and bundled SWNT devices, respectively. The inset in panel f is a comparison of the two devices (normalized to the 303 cm^{-1} Si line), showing the enhanced intensity and broadening of the G^- band in the bundled sample.

ing and selecting SWNTs of interest displayed in this work.

Complete structural information on SWNTs can be obtained from Raman analysis. Raman imaging in the form of 100-point mapping was conducted on two of the DPN-patterned device channels. The resulting spectra were compiled and averaged (dead scans on Si with no nanotube signature were discarded) and are shown in Figure 9. Figure 9c shows the Raman spectra for a semiconducting SWNT that was electrically characterized (shown in Figure 7). The single peak in the RBM region (170 cm^{-1}) indicates that this device is composed of a single semiconducting SWNT, which agrees with the AFM and electrical data. The diameter of this nanotube observed with AFM is around 1.6 ± 0.1 nm, indicating that this SWNT could have a chiral vector of either (18,2) or (14,10), which also corroborates with the RBM-determined diameter through a previously developed equation relating wavenumber to diameter for isolated SWNTs.[68] All scans from mapping on this device revealed only the 170 cm^{-1} peak (refer to Supporting Information, Figure S4). On the other hand, for the device characterized in Figure 8 showing metallic electrical behavior, the RBM region (Figure 9d) indicates average spectra with both metallic and semiconducting signatures from a SWNT bundle. In Figure 9d (and clearly seen in Supporting Information, Figure S4), a metallic RBM peak is observed centered at 200 cm^{-1}, most likely from a (12,6) metallic tube with diameter around 1.3 ± 0.1 nm. The AFM-measured height of the SWNT bundle is ~2.5 to 3 nm (approximately what is expected for a two-tube bundle). Thus, both the AFM and Raman analysis for the reported metallic SWNT device indicate that it is composed of a bundle. The peaks at ~135 cm^{-1} and ~149 cm^{-1} are noise from air.

In addition to the RBM region, the G-band region is also quite different for the two devices. Most notably, the G^--band for the bundled sample is much more intense (inset, Figure 9f) because the two tubes are resonant rather than a single SWNT. Also, this band is broader than the corresponding G^--band for the single SWNT, which has a Lorentzian shape, confirming that the single SWNT is semiconducting (clearly seen in Supporting Information, Figure S4). The peaks around 1325 cm^{-1} result from defects in nanotubes (D-band), and this peak is relatively larger for the single SWNT. Since the SWNTs were solution processed, this larger peak could be a result of the single tube becoming more damaged during sonication than the more rigid bundles. Another peak around 1440 cm^{-1} could be attributed to substrate effects[69] or possible organic (MHA) residue.[70] However, this peak has also been observed for ~1.5 nm-diameter, isolated semiconducting SWNTs in slightly bad resonance at 633 nm excitation,[71] which

could explain why it is stronger in the case of the device with the single SWNT.

CONCLUSIONS

Several parameters were studied to enable DPN patterning of functional SWNT devices. The optimal range of MHA diffusivity was found to be 0.02−0.05 μm^2/s for reliable patterning. The ferric nitrate/thiourea etchant yielded a cleaner etch and better pattern fidelity than the ferri/ferrocyanide etchant. Two different device fabrication methods were used for patterning the larger Au electrodes that contacted the MHA-masked Au. The resultant SWNT devices were comparable to those defined by electron-beam lithography; the conductivity of the MHA-masked contacts was ~4−5 × 10^6 S/m and the $I-V$ characteristics of SWNT thin-films before and after Au deposition and etching were shown to be similar. Furthermore, the measured SWNT transconductance values were on the order of $10^{-8}-10^{-9}$ S, and the field-effect mobilities were consistent with literature reports for isolated, solution-processed SWNTs. Finally, Raman spectra corroborated the SWNT characteristics obtained from AFM and electrical data and provided insight into the structure of the nanotubes comprising these devices.

DPN-patterned devices can be used to further elucidate the intrinsic electrical and structural properties of SWNTs under ambient conditions, e.g., enabling investigation of the effects of strain and surface chemistry on electrical properties of SWNTs,[72] charge transport through junctions, and the effect of selective band gap engineering for nanoelectronics. Furthermore, other inks besides MHA can be used as the masking layer to tune the electrical characteristics of carbon nanotube devices.[50] The advantages of this technique for patterning such devices include selective placement and design of electrical contacts, targeted and rapid device fabrication, and mild and facile processing conditions.

METHODS

Surface Preparation. Substrates consisted of heavily doped silicon wafers with 300-nm thermally grown oxide layers (Silicon Quest International) diced into centimeter-sized pieces. All substrates were cleaned for at least 20 min in a UV-ozone cleaner (model 42, Jelight Company, Inc.) before further surface modification. Amine functionalization of SiO_2 occurred through solution deposition of 1 vol. % aminopropyltrimethoxy silane (Gelest, Inc.) in toluene for 1 h, followed by sonication and rinsing in toluene and drying under N_2. The contact angle of the resultant amine surfaces was 68° ± 2°.

Spin Casting of Carbon Nanotubes. Solutions of arc-discharge single-walled nanotubes (average length of 1 μm) were obtained following a method described previously.[73] These carbon nanotube solutions were diluted to 1 μg/mL in NMP (*n*-methyl-2-pyrrolidone, EMD) for spin-casting, producing electrically isolated SWNTs on the substrate surface. Approximately 15 μL of the CNT solution was pipetted onto each substrate during spinning at 3000−4000 rpm (Headway Research). The substrates were then dried in a vacuum oven at 80 °C for approximately 1 h to remove residual solvent.

DPN of MHA. A thin Au film (15−17 nm) was thermally evaporated on the substrates containing SWNTs for DPN of MHA (16-mercaptohexadecanoic acid, Sigma-Aldrich) masks. Patterning (contact mode, set point 1.5−2 V) and imaging (contact and AC mode) were performed on an NSCRIPTOR DPN system (Nanoink, Inc.) at ambient temperature (26 °C ± 4 °C) and relative humidity (30−50%).

MHA was inked onto the diving-board cantilevers of type A Si_3N_4 probes (nominal spring constant 0.041 N/m) obtained from Nanoink, Inc. The AFM tips were dipped twice into 5 mM MHA in acetonitrile, once in deionized water, again into the MHA solution and finally into ethanol, with N_2 drying in between the dipping steps. MHA-inked tips were used for rapid imaging (speeds greater than 50 μm/s) of SWNTs for contact registration and patterning verification. A challenge in the DPN process was the offset of patterns by as much as 500 nm from the original InkCAD design, presumably due to a software issue. However, this problem usually was remedied by accounting for the offset in the design, for example, making the width of the patterns at least 1 μm.

Au Etching. A modified version of an acidic $Fe(NO_3)_3$/thiourea solution[74] was used for Au etching: 1:1 mixture of 26.6 mM $Fe(NO_3)_3 \cdot 9(H_2O)$ (J. T. Baker) and 40.0 mM thiourea (Alfa Aesar) in deionized water, adjusted to ~pH 2 using HCl (EMD). Au was etched under constant stirring at 120 rpm for 6−7 min at ambient temperature. The ferri/ferrocyanide etchant used for comparison studies was composed of 0.1 M $Na_2S_2O_3$, 1 M KOH, 0.01 M $K_3Fe(CN)_6$, and 0.001 M $K_4Fe(CN)_6$.[75] Au was etched under constant stirring at 120 rpm for ~14 min at ambient temperature. Substrates were then rinsed thoroughly in deionized water and dried with air.

Device Characterization. SWNT devices were imaged using Si probes obtained from Nanosensors, with nominal force constants of 42 N/m and nominal resonance frequencies of 320−330 kHz. AFM images were flattened using the Scanning Probe Image Processor (SPIP, Image Metrology A/S). Electrical measurements were conducted using a Keithley 4200 SC semiconductor analyzer. Prior to measurement, substrates containing photolithographically patterned Au electrodes were annealed on a hot plate at 290 °C for 20 min to ensure conductive Au contacts. Micro-Raman (LabRam Aramis, Horiba Jobin Yvon) spectroscopy of SWNTs was conducted at 633 nm (1.96 eV) excitation with 1800 grating at 100× magnification, resulting in a ~700 nm spot size. Excitation power through the filter was 1 mW for the 633 nm line. It was determined that an intensity higher than 5 mW could burn the nanotubes over the acquisition period. The spectra were acquired *via* 10 × 10 (100 point) mapping in the vicinity of the DPN-patterned device channel (easily visible at 100× magnification), with two spectra acquired and averaged at each point. Since most of these mapping points resulted in "dead scans" with no SWNT present, these "flat" spectra were discarded for the statistical analysis. All summarized data were normalized to the 303 cm^{-1} mode in silicon.

Acknowledgment. We thank S. Barman for providing carbon nanotube solutions, A. Sokolov for assistance with electrical measurements, and C. Bettinger for helpful discussions. W. M. Wang is supported by a Stanford Graduate Fellowship and an NSF Graduate Research Fellowship. This work was supported by the NSF-NIRT program.

Supporting Information Available: Optical image and electrical measurement of a DPN-patterned Au contact (Figure S1); electrical measurements of percolating SWNT networks before and after Au deposition and subsequent etching (Figure S2); AFM image and electrical measurement of a short-channel SWNT device (Figure S3); individual plots from a typical Raman spectral mapping experiment on the semiconducting SWNT and nan-

otube bundle (Figure S4). This material is available free of charge *via* the Internet at http://pubs.acs.org.

REFERENCES AND NOTES

1. Postma, H. W. C.; Teepen, T.; Yao, Z.; Grifoni, M.; Dekker, C. Carbon Nanotube Single-Electron Transistors at Room Temperature. *Science* **2001**, *293*, 76–79.
2. Martel, R.; Schmidt, T.; Shea, H. R.; Hertel, T.; Avouris, P. Single- and Multiwall Carbon Nanotube Field-Effect Transistors. *Appl. Phys. Lett.* **1998**, *73*, 2447–2449.
3. Tans, S. J.; Verschueren, A. R. M.; Dekker, C. Room-Temperature Transistor Based on a Single Carbon Nanotube. *Nature* **1998**, *393*, 49–52.
4. Durkop, T.; Kim, B. M.; Fuhrer, M. S. Properties and Applications of High-Mobility Semiconducting Nanotubes. *J. Phys.: Condens. Matter* **2004**, *16*, R553–R580.
5. Kong, J.; Franklin, N. R.; Zhou, C.; Chapline, M. G.; Peng, S.; Cho, K.; Dai, H. Nanotube Molecular Wires as Chemical Sensors. *Science* **2000**, *287*, 622–625.
6. Lee, C. Y.; Baik, S.; Zhang, J. Q.; Masel, R. I.; Strano, M. S. Charge Transfer from Metallic Single-Walled Carbon Nanotube Sensor Arrays. *J. Phys. Chem. B* **2006**, *110*, 11055–11061.
7. Snow, E. S.; Perkins, F. K.; Houser, E. J.; Badescu, S. C.; Reinecke, T. L. Chemical Detection with a Single-Walled Carbon Nanotube Capacitor. *Science* **2005**, *307*, 1942–1945.
8. Ishikawa, F. N.; Chang, H.-K.; Ryu, K.; Chen, P.-C.; Badmaev, A.; Gomez De Arco, L.; Shen, G.; Zhou, C. Transparent Electronics Based on Transfer Printed Aligned Carbon Nanotubes on Rigid and Flexible Substrates. *ACS Nano* **2009**, *3*, 73–79.
9. Hu, L.; Hecht, D. S.; Gruner, G. Percolation in Transparent and Conducting Carbon Nanotube Networks. *Nano Lett.* **2004**, *4*, 2513–2517.
10. Hellstrom, S. L.; Lee, H. W.; Bao, Z. Polymer-Assisted Direct Deposition of Uniform Carbon Nanotube Bundle Networks for High Performance Transparent Electrodes. *ACS Nano* **2009**, *3*, 1423–1430.
11. Javey, A.; Guo, J.; Wang, Q.; Lundstrom, M.; Dai, H. Ballistic Carbon Nanotube Field-Effect Transistors. *Nature* **2003**, *424*, 654–657.
12. Zhou, X. J.; Park, J. Y.; Huang, S. M.; Liu, J.; McEuen, P. L. Band Structure, Phonon Scattering, and the Performance Limit of Single-Walled Carbon Nanotube Transistors. *Phys. Rev. Lett.* **2005**, *95*, 146805-1–146805-4.
13. Chen, Z.; Appenzeller, J.; Knoch, J.; Lin, Y.-M.; Avouris, P. The Role of Metal-Nanotube Contact in the Performance of Carbon Nanotube Field-Effect Transistors. *Nano Lett.* **2005**, *5*, 1497–1502.
14. Dai, H.; Wong, E. W.; Lieber, C. M. Probing Electrical Transport in Nanomaterials: Conductivity of Individual Carbon Nanotubes. *Science* **1996**, *272*, 523–526.
15. Durkop, T.; Getty, S. A.; Cobas, E.; Fuhrer, M. S. Extraordinary Mobility in Semiconducting Carbon Nanotubes. *Nano Lett.* **2004**, *4*, 35–39.
16. Zhen, Y.; Postma, H. W. C.; Balents, L.; Dekker, C. Carbon Nanotube Intramolecular Junctions. *Nature* **1999**, *402*, 273–276.
17. Smith, B. W.; Luzzi, D. E. Electron Irradiation Effects in Single Wall Carbon Nanotubes. *J. Appl. Phys.* **2001**, *90*, 3509–3515.
18. Vijayaraghavan, A.; Kanzaki, K.; Suzuki, S.; Kobayashi, Y.; Inokawa, H.; Ono, Y.; Kar, S.; Ajayan, P. M. Metal-Semiconductor Transition in Single-Walled Carbon Nanotubes Induced by Low-Energy Electron Irradiation. *Nano Lett.* **2005**, *5*, 1575–1579.
19. Suzuki, S.; Kobayashi, Y. Diameter Dependence of Low-Energy Electron and Photon Irradiation Damage in Single-Walled Carbon Nanotubes. *Chem. Phys. Lett.* **2006**, *430*, 370–374.
20. Kanzaki, K.; Suzuki, S.; Inokawa, H.; Ono, Y.; Vijayaraghavan, A.; Kobayashi, Y. Mechanism of Metal-Semiconductor Transition in Electric Properties of Single-Walled Carbon Nanotubes Induced by Low-Energy Electron Irradiation. *J. Appl. Phys.* **2007**, *101*, 0343171−0343174.
21. Mølhave, K.; Gudnason, S. B.; Pedersen, A. T.; Clausen, C. H.; Horsewell, A.; Bøggild, P. Electron Irradiation-Induced Destruction of Carbon Nanotubes in Electron Microscopes. *Ultramicroscopy* **2007**, *108*, 52–57.
22. Ginger, D. S.; Zhang, H.; Mirkin, C. A. The Evolution of Dip-Pen Nanolithography. *Angew. Chem., Int. Ed.* **2004**, *43*, 30–45.
23. Salaita, K.; Wang, Y. H.; Mirkin, C. A. Applications of Dip-Pen Nanolithography. *Nat. Nanotechnol.* **2007**, *2*, 145–155.
24. Piner, R. D.; Zhu, J.; Xu, F.; Hong, S. H.; Mirkin, C. A. "Dip-Pen" Nanolithography. *Science* **1999**, *283*, 661–663.
25. Zhang, H.; Jin, R. C.; Mirkin, C. A. Synthesis of Open-Ended, Cylindrical Au−Ag Alloy Nanostructures on a Si/SiO_x Surface. *Nano Lett.* **2004**, *4*, 1493–1495.
26. Li, B.; Lu, G.; Zhou, X. Z.; Cao, X. H.; Boey, F.; Zhang, H. Controlled Assembly of Gold Nanoparticles and Graphene Oxide Sheets on Dip Pen Nanolithography-Generated Templates. *Langmuir* **2009**, *25*, 10455–10458.
27. Haaheim, J.; Eby, R.; Nelson, M.; Fragala, J.; Rosner, B.; Zhang, H.; Athas, G. Dip Pen Nanolithography (DPN): Process and Instrument Performance with Nanoink's Nscriptor System. *Ultramicroscopy* **2005**, *103*, 117–132.
28. Lim, J. H.; Mirkin, C. A. Electrostatically Driven Dip-Pen Nanolithography of Conducting Polymers. *Adv. Mater.* **2002**, *14*, 1474–1477.
29. Maynor, B. W.; Filocamo, S. F.; Grinstaff, M. W.; Liu, J. Direct-Writing of Polymer Nanostructures: Poly(thiophene) Nanowires on Semiconducting and Insulating Surfaces. *J. Am. Chem. Soc.* **2002**, *124*, 522–523.
30. Su, M.; Aslam, M.; Fu, L.; Wu, N.; Dravid, V. P. Dip-Pen Nanopatterning of Photosensitive Conducting Polymer Using a Monomer Ink. *Appl. Phys. Lett.* **2004**, *84*, 4200–4202.
31. Lee, K. B.; Lim, J. H.; Mirkin, C. A. Protein Nanostructures Formed *via* Direct-Write Dip-Pen Nanolithography. *J. Am. Chem. Soc.* **2003**, *125*, 5588–5589.
32. Lenhert, S.; Sun, P.; Wang, Y. H.; Fuchs, H.; Mirkin, C. A. Massively Parallel Dip-Pen Nanolithography of Heterogeneous Supported Phospholipid Multilayer Patterns. *Small* **2007**, *3*, 71–75.
33. Lim, J. H.; Ginger, D. S.; Lee, K. B.; Heo, J.; Nam, J. M.; Mirkin, C. A. Direct-Write Dip-Pen Nanolithography of Proteins on Modified Silicon Oxide Surfaces. *Angew. Chem., Int. Ed.* **2003**, *42*, 2309–2312.
34. Senesi, A. J.; Rozkiewicz, D. I.; Reinhoudt, D. N.; Mirkin, C. A. Agarose-Assisted Dip-Pen Nanolithography of Oligonucleotides and Proteins. *ACS Nano* **2009**, *3*, 2394–2402.
35. Zhou, X. Z.; Chen, Y. H.; Li, B.; Lu, G.; Boey, F. Y. C.; Ma, J.; Zhang, H. Controlled Growth of Peptide Nanoarrays on Si/SiO_x Substrates. *Small* **2008**, *4*, 1324–1328.
36. Wang, W. M.; Stoltenberg, R. M.; Liu, S.; Bao, Z. Direct Patterning of Gold Nanoparticles Using Dip-Pen Nanolithography. *ACS Nano* **2008**, *2*, 2135–2142.
37. Ben Ali, M.; Ondarcuhu, T.; Brust, M.; Joachim, C. Atomic Force Microscope Tip Nanoprinting of Gold Nanoclusters. *Langmuir* **2002**, *18*, 872–876.
38. Garno, J. C.; Yang, Y. Y.; Amro, N. A.; Cruchon-Dupeyrat, S.; Chen, S. W.; Liu, G. Y. Precise Positioning of Nanoparticles on Surfaces Using Scanning Probe Lithography. *Nano Lett.* **2003**, *3*, 389–395.
39. Thomas, P. J.; Kulkarni, G. U.; Rao, C. N. R. Dip-Pen Lithography Using Aqueous Metal Nanocrystal Dispersions. *J. Mater. Chem.* **2004**, *14*, 625–628.
40. Li, B.; Goh, C. F.; Zhou, X. Z.; Lu, G.; Tantang, H.; Chen, Y. H.; Xue, C.; Boey, F. Y. C.; Zhang, H. Patterning Colloidal Metal Nanoparticles for Controlled Growth of Carbon Nanotubes. *Adv. Mater.* **2008**, *20*, 4873–4878.
41. Wang, H. T.; Nafday, O. A.; Haaheim, J. R.; Tevaarwerk, E.; Amro, N. A.; Sanedrin, R. G.; Chang, C. Y.; Ren, F.; Pearton, S. J. Toward Conductive Traces: Dip Pen Nanolithography (R) of Silver Nanoparticle-Based Inks. *Appl. Phys. Lett.* **2008**, *93*, 143105-1–143105-3.

42. Zhang, H.; Li, Z.; Mirkin, C. A. Dip-Pen Nanolithography-Based Methodology for Preparing Arrays of Nanostructures Functionalized with Oligonucleotides. *Adv. Mater.* **2002**, *14*, 1472–1474.
43. Zhang, H.; Chung, S.-W.; Mirkin, C. A. Fabrication of Sub-50-nm Solid-State Nanostructures on the Basis of Dip-Pen Nanolithography. *Nano Lett.* **2002**, *3*, 43–45.
44. Lu, G.; Chen, Y. H.; Li, B.; Zhou, X. Z.; Xue, C.; Ma, J.; Boey, F. Y. C.; Zhang, H. Dip-Pen Nanolithography-Generated Patterns Used as Gold Etch Resists: A Comparison Study of 16-Mercaptohexadecanioc Acid and 1-Octadecanethiol. *J. Phys. Chem. C* **2009**, *113*, 4184–4187.
45. Zhang, H.; Amro, N. A.; Disawal, S.; Elghanian, R.; Shile, R.; Fragala, J. High-Throughput Dip-Pen-Nanolithography-Based Fabrication of Si Nanostructures. *Small* **2007**, *3*, 81–85.
46. Zhang, H.; Elghanian, R.; Amro, N. A.; Disawal, S.; Eby, R. Dip Pen Nanolithography Stamp Tip. *Nano Lett.* **2004**, *4*, 1649–1655.
47. Huo, F. W.; Zheng, Z. J.; Zheng, G. F.; Giam, L. R.; Zhang, H.; Mirkin, C. A. Polymer Pen Lithography. *Science* **2008**, *321*, 1658–1660.
48. Zhang, H.; Mirkin, C. A. DPN-Generated Nanostructures Made of Gold, Silver, and Palladium. *Chem. Mater.* **2004**, *16*, 1480–1484.
49. Yaish, Y.; Park, J. Y.; Rosenblatt, S.; Sazonova, V.; Brink, M.; McEuen, P. L. Electrical Nanoprobing of Semiconducting Carbon Nanotubes Using an Atomic Force Microscope. *Phys. Rev. Lett.* **2004**, *92*, 046401-1−046401-4.
50. Lee, C. W.; Zhang, K.; Tantang, H.; Lohani, A.; Mhaisalkar, S. G.; Li, L.-J.; Nagahiro, T.; Tamada, K.; Chen, Y. Tuning of Electrical Characteristics in Networked Carbon Nanotube Field-Effect Transistors Using Thiolated Molecules. *Appl. Phys. Lett.* **2007**, *91*, 103515-1−103515-3.
51. Delamarche, E.; Michel, B.; Kang, H.; Gerber, C. Thermal Stability of Self-Assembled Monolayers. *Langmuir* **2002**, *10*, 4103–4108.
52. Yuan, M.; Zhan, S.; Zhou, X.; Liu, Y.; Feng, L.; Lin, Y.; Zhang, Z.; Hu, J. A Method for Removing Self-Assembled Monolayers on Gold. *Langmuir* **2008**, *24*, 8707–8710.
53. Heinze, S.; Tersoff, J.; Martel, R.; Derycke, V.; Appenzeller, J.; Avouris, P. Carbon Nanotubes as Schottky Barrier Transistors. *Phys. Rev. Lett.* **2002**, *89*, 106801-1–106801-4.
54. Wei, J. H.; Ginger, D. S. A Direct-Write Single-Step Positive Etch Resist for Dip-Pen Nanotithography. *Small* **2007**, *3*, 2034–2037.
55. Saalmink, M.; van der Marel, C.; Stapert, H. R.; Burdinski, D. Positive Microcontact Printing with Mercaptoalkyloligo-(ethylene glycol)s. *Langmuir* **2006**, *22*, 1016–1026.
56. Selvarasah, S.; Chao, S. H.; Chen, C. L.; Sridhar, S.; Busnaina, A.; Khademhosseini, A.; Dokmeci, M. R. A Reusable High Aspect Ratio Parylene-C Shadow Mask Technology for Diverse Micropatterning Applications. *Sens. Actuators, A* **2008**, *145*−*146*, 306–315.
57. Zhang, Q. G.; Cao, B. Y.; Zhang, X.; Fujii, M.; Takahashi, K. Influence of Grain Boundary Scattering on the Electrical and Thermal Conductivities of Polycrystalline Gold Nanofilms. *Phys. Rev. B* **2006**, *74*, 134109-1–134109-5.
58. Kim, W. J.; Lee, C. Y.; O'Brien, K. P.; Plombon, J. J.; Blackwell, J. M.; Strano, M. S. Connecting Single Molecule Electrical Measurements to Ensemble Spectroscopic Properties for Quantification of Single-Walled Carbon Nanotube Separation. *J. Am. Chem. Soc.* **2009**, *131*, 3128–3129.
59. Collins, P. G.; Arnold, M. S.; Avouris, P. Engineering Carbon Nanotubes and Nanotube Circuits Using Electrical Breakdown. *Science* **2001**, *292*, 706–709.
60. Yao, Z.; Kane, C. L.; Dekker, C. High-Field Electrical Transport in Single-Wall Carbon Nanotubes. *Phys. Rev. Lett.* **2000**, *84*, 2941–2944.
61. Wilder, J. W. G.; Venema, L. C.; Rinzler, A. G.; Smalley, R. E.; Dekker, C. Electronic Structure of Atomically Resolved Carbon Nanotubes. *Nature* **1998**, *391*, 59–62.
62. Odom, T. W.; Huang, J.-L.; Kim, P.; Lieber, C. M. Atomic Structure and Electronic Properties of Single-Walled Carbon Nanotubes. *Nature* **1998**, *391*, 62–64.
63. Tsang, J. C.; Freitag, M.; Perebeinos, V.; Liu, J.; Avouris, P. Doping and Phonon Renormalization in Carbon Nanotubes. *Nat. Nanotechnol.* **2007**, *2*, 725–730.
64. Yuan, S.; Zhang, Q.; You, Y.; Shen, Z.-X.; Shimamoto, D.; Endo, M. Correlation between *in Situ* Raman Scattering and Electrical Conductance for an Individual Double-Walled Carbon Nanotube. *Nano Lett.* **2008**, *9*, 383–387.
65. Fanchini, G.; Unalan, H. E.; Chhowalla, M. Voltage-Induced Dependence of Raman-Active Modes in Single-Wall Carbon Nanotube Thin Films. *Nano Lett.* **2007**, *7*, 1129–1133.
66. Wang, C.; Cao, Q.; Ozel, T.; Gaur, A.; Rogers, J. A.; Shim, M. Electronically Selective Chemical Functionalization of Carbon Nanotubes: Correlation between Raman Spectral and Electrical Responses. *J. Am. Chem. Soc.* **2005**, *127*, 11460–11468.
67. Jiao, L.; Xian, X.; Wu, Z.; Zhang, J.; Liu, Z. Selective Positioning and Integration of Individual Single-Walled Carbon Nanotubes. *Nano Lett.* **2008**, *9*, 205–209.
68. Jorio, A.; Saito, R.; Hafner, J. H.; Lieber, C. M.; Hunter, M.; McClure, T.; Dresselhaus, G.; Dresselhaus, M. S. Structural (*n*, *m*) Determination of Isolated Single-Wall Carbon Nanotubes by Resonant Raman Scattering. *Phys. Rev. Lett.* **2001**, *86*, 1118–1121.
69. Souza Filho, A. G.; Jorio, A.; Swan, A. K.; Ünlü, M. S.; Goldberg, B. B.; Saito, R.; Hafner, J. H.; Lieber, C. M.; Pimenta, M. A.; Dresselhaus, G.; Dresselhaus, M. S. Anomalous Two-Peak G′-Band Raman Effect in One Isolated Single-Wall Carbon Nanotube. *Phys. Rev. B* **2002**, *65*, 085417−1−085417−8.
70. Knief, P.; Clarke, C.; Herzog, E.; Davoren, M.; Lyng, F. M.; Meade, A. D.; Byrne, H. J. Raman Spectroscopy—A Potential Platform for the Rapid Measurement of Carbon Nanotube-Induced Cytotoxicity. *Analyst* **2009**, *134*, 1182–1191.
71. Jorio, A.; Pimenta, M. A.; Souza Filho, A. G.; Saito, R.; Dresselhaus, G.; Dresselhaus, M. S. Characterizing Carbon Nanotube Samples with Resonance Raman Scattering. *New J. Phys.* **2003**, *5*, 139.
72. Minot, E. D.; Yaish, Y.; Sazonova, V.; Park, J. Y.; Brink, M.; McEuen, P. L. Tuning Carbon Nanotube Band Gaps with Strain. *Phys. Rev. Lett.* **2003**, *90*, 156401-1–156401-4.
73. LeMieux, M. C.; Roberts, M.; Barman, S.; Jin, Y. W.; Kim, J. M.; Bao, Z. Self-Sorted, Aligned Nanotube Networks for Thin-Film Transistors. *Science* **2008**, *321*, 101–104.
74. Geissler, M.; Wolf, H.; Stutz, R.; Delamarche, E.; Grummt, U. W.; Michel, B.; Bietsch, A. Fabrication of Metal Nanowires Using Microcontact Printing. *Langmuir* **2003**, *19*, 6301–6311.
75. Weinberger, D. A.; Hong, S. G.; Mirkin, C. A.; Wessels, B. W.; Higgins, T. B. Combinatorial Generation and Analysis of Nanometer- and Micrometer-Scale Silicon Features *via* "Dip-Pen" Nanolithography and Wet Chemical Etching. *Adv. Mater.* **2000**, *12*, 1600–1603.